Atmos. Chem. Phys. Discuss., 10, 30305–30345, 2010
www.atmos-chem-phys-discuss.net/10/30305/2010/
doi:10.5194/acpd-10-30305-2010

Atmospheric Chemistry and Physics Discussions

A minimum bulk microphysics

J.-I. Yano and D. Bouniol

GAME/CNRS, CNRS-INSU-Météo France, URA 1357, Toulouse, France

Received: 2 September 2010 – Accepted: 27 October 2010 – Published: 13 December 2010

Correspondence to: J.-I. Yano (jun-ichi.yano@zmaw.de)

Published by Copernicus Publications on behalf of the European Geosciences Union.

Abstract

Cloud microphysics present extreme complexities, and even under bulk approaches, the formulation tends to be involved. A minimum microphysics is proposed, aimed at applications for geophysical fluid dynamics, by a maximum simplification of a standard bulk formulation. The proposed formulation is also independently derived by a simple phenomenological argument. The formulational structure of the bulk microphysics is also discussed. The autoconversion process formulation is discussed separately in a phenomenological manner, because a formal application of the bulk approach becomes involved. Four major possible formulations for autoconversion are identified. The proposed formulation is tested with a nonhydrostatic anelastic model under segmentally-constant approximation (NAM-SCA).

1 Introduction

Tropical convective dynamics can be considered as a fascinating theoretical problem containing many aspects that geophysical fluid dynamics as well as applied mathematics can greatly contribute. Especially in the large-scale limit, for example, the approach of an asymptotic expansion appears to provide a good description of the interactions between deep convection and large-scale circulations. The contributions of Andrew J. Majda and his colleagues in recent years may be cited as a particular example (e.g., Biello et al., 2007; Khouider and Majda, 2006, 2007; Majda, 2007a,b).

However, a serious obstacle in pursuing these theoretical approaches for tropical convective dynamics is the extreme complexity of cloud microphysics associated with these convective processes. The literature is extensive (e.g., Pruppacher and Klett, 1997), and the more compact of the textbooks (e.g., Rogers and Yau, 1989) give an impression that they do not cover a great deal compared to some recently-developed sophisticated microphysics models (e.g., Phillips et al., 2001; Khain et al., 2004; Morrison et al., 2005). The present study represents an attempt to present the existing

ACPD
10, 30305–30345, 2010

microphysics models in a general perspective.

Simple formulations for microphysics are provided in terms of the bulk approach, an approach that may be traced back to Kessler (1965, 1969). However, from an applied mathematical point of view, such as that taken in asymptotic expansion theories, even these bulk formulations are still too involved in order to allow a theoretical analysis. Also in the climate modelling context, a simplest-possible microphysics may be sufficient for certain applications (cf., Held, 2005).

The goal of the present paper is to propose a much simpler bulk microphysics formulation that can be adopted for theoretical studies as well as *idealized* climate studies. We call the proposed formulation *a minimum bulk microphysics*.

The present work is partially inspired by Grabowski (1998), who proposes a coherent framework for a simple microphysics, including ice, suitable for studies of interactions between convection and the large-scale dynamics in the climate context. Unfortunately, in the opinion of the first author, the proposed formulation is, nevertheless, still too complex. A further simplification is attempted in the present paper, more from an applied mathematics point of view. In order to achieve maximum simplicity, even ice microphysics are not considered. In the following description, we simply assume that water never freezes (i.e., it remains in a supercooled state) even below the freezing point.

The paper is organized as follows. The next section provides an overview of the microphysical processes to be considered, and summarizes the proposed *minimum bulk microphysics* formulation. Sect. 3 is devoted to a formal derivation of the proposed minimum microphysics. Sect. 3.1 reviews the basic idea of the bulk microphysics formulation, Sect. 3.2 derives a precise formulation for conversion terms based on the bulk formulation, and Sect. 3.3 introduces approximations of the derived formulae that lead to the proposed *minimum* formulation. Readers may skip this section, if the derivation is not their concern.

A special attention is paid to the autoconversion process (cf., Fig. 1 below), and it is treated separately in Sect. 4. As discussed in the beginning of Sect. 4, a closed expression under a formal application of the bulk microphysics approach turns out to

ACPD
10, 30305–30345, 2010

be difficult. For this reason, we take a phenomenological approach, and propose possible formulations from this perspective. The developed formulations are tested by implementing them into a nonhydrostatic anelastic model under segmentally-constant approximation (NAM-SCA) developed by the first author (Yano et al., 2010), along with the other parts of the minimum bulk microphysics. Results from these test are discussed in Sect. 5. The paper is concluded in Sect. 6.

2 Proposed minimum bulk microphysics

2.1 Overview: basic physics

The present paper considers three water types: the water vapor q_v, the cloud water q_c, and the precipitating (rain) water q_p. Each water type is described in terms of its mixing ratio.

Water is converted from one type to another by various processes. As a minimum bulk microphysics, we propose to consider the processes schematically represented in Fig. 1: water vapor q_v is converted into the cloud water q_c by condensation (CON). The cloud water q_c is then converted into precipitating water q_p by two processes. The first (autoconversion, AUT) primarily refers to the process that the cloud water converts into precipitating water through mutual collisions. The second (accretion, ACC, or collection) refers to the process that the precipitating water grows in size by accreting (or "collecting") the surrounding cloud water as its falls. The generated precipitating water q_p either precipitates out (PRC) or re-evaporates (EVP) into water vapor q_v. Note that all the physical processes are given in terms of a conversion rate per unit time, except for the precipitation rate (PRC), which is given in terms of a vertical flux (cf., Eq. 2.1d below).

ACPD
10, 30305–30345, 2010

2.2 Formulation: summary

The proposed minimum bulk microphysics are mathematically formulated by considering the following set of equations:

$$\frac{D}{Dt}\theta = \frac{L_v\bar{\theta}}{C_p\bar{T}}(CON - EVP) + F_{1,LS}, \tag{2.1a}$$

$$\frac{D}{Dt}q_v = -CON + EVP + F_{2,LS}, \tag{2.1b}$$

$$\frac{D}{Dt}q_c = CON - AUT - ACC, \tag{2.1c}$$

$$\frac{D}{Dt}q_p + \frac{1}{\bar{\rho}}\frac{\partial}{\partial z}\bar{\rho}PRC = AUT + ACC - EVP. \tag{2.1d}$$

Here, θ is the potential temperature; D/Dt designates a Lagrangian time derivative; $\bar{\rho}$, $\bar{\theta}$, and $\bar{T}$ are reference profiles for the air density, the potential temperature, and the temperature, respectively, as introduced under an anelastic approximation; $L_v = 2.5008 \times 10^6$ J/kg and $C_p = 1.0047089 \times 10^3$ J/kg/K are, respectively, the latent heat of condensation and the specific heat at constant pressure. For the latter, a value for the dry atmosphere is given as adopted in implementation in Sect. 5.

The right-hand side of Eq. (2.1) contains conversion terms associated with the microphysics, that are explained in the following. We furthermore add "large-scale" forcing, $F_{1,LS}$ and $F_{2,LS}$, to the potential temperature and the water vapor equations when testing the proposed microphysics scheme in Sect. 5.

Condensation is performed whenever the water vapor at a given grid point is supersaturated (i.e., $q_v - q_v^*(\bar{\rho},T) > 0$), and the rate, CON, is defined by a tendency over a time step Δt as

$$CON\Delta t = [q_v - q_v^*(\bar{\rho},T)]\{1 + \frac{L_v^2}{C_pR_v}\frac{q_v^*(\bar{\rho},T)}{T^2}\}^{-1}, \tag{2.2}$$

ACPD
10, 30305–30345, 2010

where $q_v^*(\bar{\rho},T)$ is the saturated water-vapor mixing ratio (at the density $\bar{\rho}$ and the temperature T), and R_v the gas constant for water vapor. Condensation based on Eq. (2.2) is also performed even under sub-saturation (i.e., $q_v - q_v^*(\bar{\rho},T) < 0$), whenever cloud-water is present (and $q_c > CON\Delta t$). In this case, the condensation rate is negative, leading to cloud evaporation, and it maintains the cloudy environment as saturated.

The formula (2.2) is divided by a nontrivial factor in order to ensure conservation of enthalpy during the condensation process over a time step Δt. The formula was derived in Asai (1965), and adopted by Yau and Austin (1979), Rutledge and Hobbs (1983), Grabowski(1988; 1989), and many others.

The evaporation rate EVP of precipitating water is given by

$$EVP = \begin{cases} \dfrac{1}{\tau_{EVP}} \dfrac{q_v^* - q_v}{q_v^*} & T > 273\mathrm{K} \\ 0 & T \le 273\mathrm{K} \end{cases} \tag{2.3}$$

with a relaxation time τ_{EVP}, which is estimated to be in the range of $\tau_{EVP} = 10^4$–10^5 s. In the present application, we set $\tau_{EVP} = 10^4$ sec. Note that due to the nondimensionality of the mixing ratio, the actual relaxation time scale is given by $q_v^*\tau_{EVP} \simeq 10^2$–$10^3$ s with $q_v^* \sim 10^{-2}$. The formula says that the re-evaporation is suppressed below the freezing point so that supercooled rain reaches the surface without re-evaporation. This rather unintuitive assumption is introduced by examining the actual temperature dependence of τ_{EVP} in Sect. 3.3.3.

The autoconversion rate, AUT, may be represented in various different ways based on phenomenological arguments. These possibilities are discussed separately in Sect. 4.

The accretion ACC of cloud water by precipitating water is proportional to the availability of both the cloud water q_c and the precipitating water q_p, if an exact collision formula (cf., Eq. 3.20 below) is applied in a bulk manner. Thus,

$$ACC = \bar{\rho}(ACC)_0 q_c q_p \tag{2.4}$$

ACPD
10, 30305–30345, 2010

with a proportionality constant $(ACC)_0 = 1.773\,\mathrm{m}^3/\mathrm{kg/sec}$. The constant is defined from an exact formula in Sect. 3.2.2.

Including an air-density factor in the definition of *ACC* may be less obvious, but arises because the rate of generation of precipitating-water content (mass per volume) $\bar{\rho}q_p$ is proportional to both precipitating-water content $\bar{\rho}q_p$ and cloud-water content $\bar{\rho}q_c$ under the bulk argument. Eq. (2.4) is obtained by dividing this formula by $\bar{\rho}$.

Finally the precipitation rate is given by

$$PRC = q_p v_T \tag{2.5}$$

with a constant rainfall velocity, that we set as $v_T = 5\,\mathrm{m/s}$. Note that the formula is based on a simple geometrical consideration on rain flux.

3 A formal basic bulk formulation

3.1 Basic premise for the bulk approach

In this section, we focus on the microphysical processes (precipitation, accretion, and re-evaporation) driven by precipitating water. The autoconversion process, which is controlled by collisions of cloud water drops, is considered separately in the next section. Under this focus, we introduce the bulk microphysics formulation in as formal manner as possible, beginning from its basic idea. Then the formulation presented in Sect. 2.2 will be iderived in a stepwise manner. Numerical values for the parameters are listed separately in Appendix A.

Within clouds, the precipitating-water drops are found in various sizes. Thus, the most legitimate approach would be to consider them in terms of the time evolution of each size category, by introducing a distribution $n_p(D)$ for the drop diameter D, or more generally, an effective size when the particle shape is not spherical. An equation for the precipitating-water drop-size distribution may be written down by considering each conversion process $C(D)$ for a given drop size D. This formulation is also legitimate

ACPD
10, 30305–30345, 2010

in the sense that formulae for $C(D)$ for each conversion processes are relatively easy to write down. However, the resulting system of equations is extensive, because the calculations must be performed for each drop-size category at each time step.

The basic idea of the bulk approach is to, somehow, circumvent this computational complexity by only considering the "total" mixing ratio for precipitating water. The size distribution $n_p(D)$ for precipitating water must also be, somehow, taken into account, at least implicitly, so that all the conversion rates can be correctly evaluated.

The reader should keep in mind that only the size distribution $n_p(D)$ for precipitating water is being considered in this section. Issues relating to the size distribution $n_c(D)$ of cloud water will be discussed in the next section separately.

Once a size distribution $n_p(D)$ of the precipitating water is specified as a function of the particle diameter D, then the "total" precipitating-water mixing ratio is given by

$$q_p = \frac{1}{\bar{\rho}} \int_0^{+\infty} n_p(D) m_p(D) dD, \tag{3.1}$$

where $m_p(D)$ is the mean mass of a precipitating-water particle with a diameter D.

The main premise of the bulk microphysical approach is to circumvent the problem of calculating the evolution of the particle size distribution with time by assuming a fixed from of the size distribution $n_p(D)$ for precipitating water. Note that the size distribution itself may evolve with time through the evolution of a time-dependent parameter in the expression for the size distribution, as explained immediately below.

A standard choice, as adopted here, is a distribution originally proposed by Marshall and Palmer (1948) based on their observational measurements:

$$n_p(D) = n_0 \exp(-\lambda D) \tag{3.2}$$

with constants n_0 and λ. The distribution has the advantage of enabling the use of Gamma function $\Gamma(x)$ to evaluate the integrals such as (3.1). The basic properties of the Gamma function are listed in Appendix B.

ACPD
10, 30305–30345, 2010

Being consistent with the observational finding by Marshall and Palmer (1948), we fix n_0 with time (cf., Appendix A1), and then set the other parameter λ is to enforce a consistency with the precipitating-water mixing ratio q_p prognostically determined by Eq. (2.1d), as shown below (cf., Eq. 3.8). In other words, the distribution slope changes with time by following the evolution of the total precipitating water.

Integration of Eq. (3.2) over D gives a total drop number

$$N_0 = \int_0^{+\infty} n_p(D) dD = \frac{n_0}{\lambda}, \tag{3.3}$$

and a similar integral multiplied by D provides the mean radius of the precipitating drops:

$$\bar{D} = \int_0^{+\infty} D n_p(D) dD = \frac{1}{\lambda}. \tag{3.4}$$

The mean mass of drops with a diameter D may be given by

$$m_p(D) = \tilde{m} D^b$$

with $\tilde{m} = \pi \rho_w / 6$ and $b = 3$. Here, ρ_w is the density of liquid water. As it turns out, for performing integrals it is convenient to introduce a constant (with respect to D) defined by $m_0 = \tilde{m} \lambda^{-b}$. Thus, we set

$$m_p(D) = m_0 (\lambda D)^b. \tag{3.5}$$

By substituting Eq. (3.2) and (3.5) into the integrand in Eq. (3.1), we obtain

$$n_p(D) m_p(D) = n_0 m_0 (\lambda D)^b \exp(-\lambda D). \tag{3.6}$$

The above equation (3.6) can be immediately integrated with the help of Eq. (B.2) from Appendix B, and we obtain

$$q_p = \frac{n_0 m_0}{\bar{\rho} \lambda} \Gamma(b+1). \tag{3.7}$$

ACPD
10, 30305–30345, 2010

By further substituting $m_0 = \tilde{m}\lambda^{-b}$ into Eq. (3.7), the parameter λ is given in terms of the precipitating-water mixing ratio as

$$\lambda = [\frac{n_0 \tilde{m}}{\bar{\rho} q_p} \Gamma(b+1)]^{1/(b+1)}. \tag{3.8}$$

Note that the mean size of the precipitation particles (Eq. 3.4) is also related to the precipitating-water mixing ratio by

$$\bar{D} = [\frac{\bar{\rho}}{n_0 \tilde{m} \Gamma(b+1)}]^{1/(b+1)} q_p^{1/(b+1)}, \tag{3.9}$$

and thus the mean raindrop size increases monotonically with a $1/(b+1)$-th power of the precipitating-water mixing ratio. By furthermore substituting $b = 3$, we find

$$\bar{D} \propto q_p^{1/4}.$$

In this manner, all the parameters related to the precipitating-water size distribution (Marshall-Palmer distribution) are determined once the precipitating-water mixing ratio, q_p, is known. That is the basic premise of the bulk microphysics approach.

3.2 A bulk formulation for precipitating-water driven processes

Rates of precipitating-water driven processes, such as the precipitating rate (PRC), accretion (ACC), and re-evaporation (EVP), can be derived by following a similar procedure as for determining the precipitating-water mixing ratio, q_p, from given distribution parameters.

In general, a bulk rate Π (given in unit of m/sec for PRC, 1/sec for ACC and EVP) for any precipitating-water driven microphysical process, under the given size distribution (Eq. 3.2), is written in terms of a corresponding rate $C(D)$ of the same microphysical

ACPD
10, 30305–30345, 2010

process for an individual precipitating-water particle with a diameter D by

$$\Pi = \int_0^{+\infty} n_p(D) C(D) dD. \tag{3.10}$$

As seen below for specific processes, the individual rate is often in a power law of the particle size D, i.e.,

$$C(D) = C_0 (\lambda D)^{\kappa} \tag{3.11}$$

with constants C_0 and κ, and a certain λ–dependence being expected for the former, say

$$C_0 = \tilde{C} \lambda^{-\nu}$$

with ν and $\tilde{C}$ unspecified constants.

Substitution of Eqs. (3.11) and (3.2) into Eq. (3.10) shows that the integrand is given by

$$n_p(D) C(D) = n_0 C_0 (\lambda D)^{\kappa} \exp(-\lambda D).$$

Thus, again, the integral can be performed by using Eq. (B.2), and we obtain

$$\Pi = \frac{n_0 \tilde{C}}{\lambda^{(\nu+1)}} \Gamma(\kappa + 1). \tag{3.12}$$

Hence, once the rate $C(D)$ for an individual particle is known in the form of Eq. (3.11) for a given microphysical process, the bulk rate (Eq. 3.10) is given by Eq. (3.12). Recall that λ is related to q_p by Eq. (3.8). Thus its substitution into Eq. (3.12) provides a dependence of the rate Π on the precipitating-water mixing ratio q_p:

$$\Pi \propto \lambda^{-(\nu+1)} \propto q_p^{(\nu+1)/(b+1)}.$$

Here we see the basic principle for the bulk microphysical formulation: the bulk rate is evaluated solely in terms of the precipitating-water mixing ratio q_p without explicitly evaluating the size distribution.

ACPD
10, 30305–30345, 2010

Note that instead of taking the above formal approach, a cruder approach may be taken, in which the integrand $C(D)$ in Eq. (3.10) is approximated by a value $C(\bar{D})$ for the mean particle size $\bar{D}$. This leads to

$$\Pi \simeq N_0 C_0, \tag{3.13}$$

where $N_0 = n_0/\lambda$ is the total number of the particles. This approximation is partially adopted by Grabowski (1998: see his Eqs. 11a, b). We see by comparing Eqs. (3.12) and (3.13) that this approximation leads to an error of a factor $\Gamma(\kappa+1)$. Importantly, there is no error when $\kappa = 1$, and the error is small so long as the parameter is close to $\kappa = 1$. However, in general, we should expect an error of a finite factor.

In the following, by applying this formal bulk principle, explicit formulae for the precipitation rate (PRC), accretion (ACC), and re-evaporation (EVP) are derived.

3.2.1 Precipitation

The total precipitation rate PRC is given by

$$PRC = \frac{1}{\bar{\rho}} \int_0^{+\infty} n_p(D) prc(D) dD \tag{3.14}$$

The precipitation rate $prc(D)$ for an individual particle is proportional to both the fall velocity (terminal velocity) $v_T(D)$ of a precipitating particle and its typical mass $m_p(D)$, thus

$$prc(D) = m_p(D) v_T(D), \tag{3.15}$$

where the fall velocity is typically given by

$$v_T(D) = \tilde{v} D^d \tag{3.16}$$

with constants $\tilde{v}$ and d.

ACPD
10, 30305–30345, 2010

By substituting Eqs. (3.5), (3.15), and (3.16) into Eq. (3.14), we obtain

$$PRC = q_p v_T^*, \tag{3.17}$$

where

$$v_T^* = \frac{\Gamma(b+d+1)}{\Gamma(b+1)} \frac{\tilde{v}}{\lambda^d} = \tilde{v} \frac{\Gamma(b+d+1)}{\Gamma(b+1)} \left[\frac{\bar{\rho} q_p}{n_0 \tilde{m} \Gamma(b+1)}\right]^{d/(b+1)} \tag{3.18}$$

is the mean fall velocity of precipitating water.

3.2.2 Accretion

The total accretion rate ACC is given by

$$ACC = \int_0^{+\infty} n_p(D) acc(D) dD. \tag{3.19}$$

The rate $acc(D)$ that an individual precipitating-water particle accretes ("collects") surrounding cloud water is defined in terms of the volume $\Sigma v_T(D)$ of air swept by a precipitating particle per unit time and the availability of cloud water per volume (here measured by cloud-water mixing ratio), as well as the collection efficiency E (Appendix A3), thus

$$acc(D) = E \Sigma v_T(D) q_c \tag{3.20}$$

where

$$\Sigma = \alpha \frac{\pi}{4} D^2 \tag{3.21}$$

is the sweeping section with a constant α. For a spherical particle $\alpha = 1$.

By substituting Eqs. (3.16) and (3.21) into Eq. (3.20), Eq. (3.19) can be integrated, which gives

$$ACC = (ACC)_0 (\bar{\rho} q_p)^{(d+3)/(b+1)} q_c \tag{3.22}$$

with

$$(ACC)_0 = \frac{\pi}{4} E \alpha c n_0 \frac{\Gamma(d+3)}{[n_0 \tilde{m} \Gamma(b+1)]^{(d+3)/(b+1)}}. \tag{3.23}$$

ACPD
10, 30305–30345, 2010

3.2.3 Re-evaporation

The re-evaporation rate EVP is given by

$$EVP = \frac{1}{\bar{\rho}} \int_0^{+\infty} n_p(D) evp(D) dD, \tag{3.24}$$

where the re-evaporation rate $evp(D)$ for an individual precipitating particle is given by

$$evp(D) = 4\pi C(1 - RH) FG(p,T). \tag{3.25}$$

Here, $C = D/\beta$: particle capacitance
$RH = q_v/q_v^*$: relative humidity
$F = F_0 + \psi Re^{1/l}$: ventilation factor
$G(p,T)$: thermodynamic function
The parameters introduced in the above list are:
$\beta = 2$: precipitation particle geometry
$Re = \bar{\rho} D v_T(D)/\mu$: Reynolds number, where v_T is defined by Eq. (3.16).
$\mu = 1.72 \times 10^{-5}$ Ns/m^2: dynamic viscosity of air
F_0, ψ, and l are the constants defined in Appendix A4.
The thermodynamic function $G(T)$ above is defined by

$$G(T) = [\frac{R_v T}{D_v e^*(T)} + \frac{L_e}{kT}(\frac{L_e}{R_v T} - 1)]^{-1}, \tag{3.26}$$

where $e^*(T)$ is the saturated water-vapor pressure at the given temperature T, and D_v is the diffusion coefficient for the water vapor. Grabowski (1998) adopts an approximation

$$G(T) = A(2.2\frac{T}{e^*(T)} + \frac{2.2 \times 10^2}{T})^{-1}, \tag{3.27}$$

ACPD
10, 30305–30345, 2010

where $A = 10^{-7}$ kg/m/s. For a derivation of Eq. (3.25), refer to e.g., Ch. 13 of Pruppacher and Klett (1997), Ch. 7 of Rogers and Yau (1989), and Yano (2010).

By substituting the definitions of the Reynolds number and Eq. (3.16) into the definition of the ventilation factor,

$$F = F_0 + \psi Re^{1/l}$$

$$= F_0 + (\frac{\bar{\rho} v_0}{\lambda})^{1/2} \psi (\lambda D)^{(d+1)/2l}.$$

Further substitution into Eq. (3.25) provides

$$evp(D) = \frac{1}{\lambda} \frac{4\pi}{\beta} (1 - RH) G(T) \{\lambda F_0 D + \psi (\frac{\rho v_0}{\lambda \mu})^{1/2} (\lambda D)^{(d+1)/2l+1}\}. \quad (3.28)$$

Note that Eq. (3.28) consists of a sum of two terms, each of which is analogous to Eq. (3.11). Thus the expression is integrable analytically using Eq. (B.2).

Substituting Eq. (3.28) into Eq. (3.24) and performing the integral, we obtain

$$EVP = \frac{4\pi n_0}{\beta \bar{\rho}} \bar{D}^2 (1 - RH) G(T) \tilde{F}, \quad (3.29)$$

where the bulk ventilation factor $\tilde{F}$ is defined by

$$\tilde{F} = F_0 + \psi (\bar{\rho} c / \mu)^{1/2} (\frac{\bar{\rho} q_p}{n_0 \tilde{m} \Gamma(b+1)})^{(d+1)/2(b+1)} \Gamma(\frac{d+1}{2l} + 2). \quad (3.30)$$

3.3 Further simplifications

The formulae obtained by a strict application of the bulk approach in the last subsection appear to be rather involved. In this subsection, we attempt further simplifications by analyzing these formulae.

ACPD
10, 30305–30345, 2010

3.3.1 Terminal velocity in precipitation rate

The definition of the precipitation rate given by Eq. (3.17) is concise and lucid, except for the formula (3.18) for the terminal velocity of precipitating water, which is rather involved. In order to examine it, Eq. (3.18) is plotted as a function of the precipitating-water mixing ratio q_p in Fig. 2 with the surface air density, $\bar{\rho} = 1\,\mathrm{kg/m^3}$. It is seen that the terminal velocity v_T changes only slowly (by factors of a few) when the precipitating-water mixing ratio q_p is changed over orders of magnitude. This suggests that for simple modelling, the terminal velocity may be taken as a constant, as assumed in Eq. (2.5).

3.3.2 Accretion

The standard parameters given in Appendix A3 suggest that

$$\frac{d+3}{b+1} \simeq 1$$

is a good approximation. Under this approximation, the accretion formula (Eq. 3.22) reduces to Eq. (2.4). Note that Eq. (2.4) takes the same form as the one expected for an individual particle of size D:

$$n_p(D)acc(D) \propto n_p(D)q_c$$

(cf., Eqs. 3.19 and 3.20). This approximation is also adopted by Lopez (2002).

3.3.3 Re-evaporation

In order to present the re-evaporation rate given by Eq. (3.29) in a simpler format, we have proposed to take a linear relaxation formula (2.3). Comparison between Eqs. (2.3) and (3.29) indicates that the relaxation time is defined by

$$\tau_{EVP} = \frac{\bar{\rho}\beta}{4\pi n_0 \bar{D}^2}(G(T)\tilde{F})^{-1}. \tag{3.31}$$

ACPD
10, 30305–30345, 2010

In order to seek a simple expression for Eq. (3.31), we, first note that for a range of precipitating-water mixing ratios, $q_p = 10^{-2}$–10 g/kg, the Reynolds number Re spans the range 10–100. This translates into a variation of the ventilation factor $\tilde{F}$ =1–10. Next, the thermodynamic function $G(T)$ defined by Eq. (3.26) is plotted in Fig. 3 as a function of the temperature, T. It is seen that $G(T)$ rapidly approaches zero below, say, the freezing point of $T = 273$K. We propose to take a step function for approximating this function:

$$G(T) \simeq \begin{cases} A & T > 273\text{K} \\ 0 & T \leq 273\text{K} \end{cases} \tag{3.32}$$

with a constant $A = 10^{-7}$ kg/m/s. Finally, the remaining factors in Eq. (3.31) are estimated as

$$\bar{\rho}\left(\frac{\beta}{4\pi}\right)\frac{1}{n_0 \bar{D}^2} = 1\text{kg/m}^3/10 \times 10^{-7+3\times 2} = 10^{-2}\text{kg/m}$$

with $\bar{\rho} = 1\text{kg/m}^3$, $4\pi/\beta \simeq 10$, $n_0 = 10^7\text{m}^{-4}$, $\bar{D} = 10^{-3}$m. After combining all these results together,

$$\tau_{EVP} = \begin{cases} 10^4\text{–}10^5\text{s} & T > 273\,\text{K} \\ \infty & T \leq 273\text{K}. \end{cases}$$

In a more general case, however, if ice is also included, then the approximation (3.32) is not acceptable for the following reason. Due to the difference between the saturated water-vapor pressure for water and ice, ice can easily reach much higher supersaturations than water, with the ratio of $(\text{RH}_{\text{ice}} - 1)/(\text{RH}_{\text{water}} - 1)$ reaching up to 10^3. As a result, the small but finite value for $G(T)$ below freezing point must be explicitly taken into account for ice (W. W. Grabowski, personal communication, 2008).

4 Phenomenology for autoconversion

Autoconversion refers to the process through which precipitating-water drops form by a series of coalescence of cloud-water drops. Generally, by analogy with the way that

ACPD
10, 30305–30345, 2010

accretion is formulated in Sect. 3.2.2, the autoconversion rate can be evaluated by

$$AUT = \int_0^\infty \int_0^\infty k(D_1, D_2) n_c(d_1) n_c(D_2) dD_1 dD_2, \tag{4.1}$$

where $k(D_1, D_2)$ is a rate (probability) that precipitating water is generated by a coalescence of two could-water drops with the diameters D_1 and D_2. A total generation rate of precipitating water is obtained by integrating the contribution from all of the possible diameters for D_1 and D_2 as defined by Eq. (4.1). Here, $n_c(D)$ is the number density of the cloud water with a diameter D.

Unfortunately, it is difficult to derive an analytical expression for the autoconversion rate starting from Eq. (4.1) for several reasons. First of all, the double integral defined by Eq. (4.1) is more difficult to perform than a single integral defined by Eq. (3.10) for the precipitating-water driven processes. More importantly, the from of the kernel, $k(D_1, D_2)$, is still controversial partially due to the fact that the autoconversion rate is sensitive to complex flows surrounding cloud-water drops. See e.g., Ch. 15 of Pruppacher and Klett (1997), Seifert and Beheng (2001) for detailed discussions.

For these reasons, in this section, we instead pursue a phenomenological description of the autoconversion process. Recall that Kessler (1965, 1969) also introduced his autoconversion formulation on a purely phenomenological basis. The present section extends more this line of arguments into a general perspective. Kessler's (1965, 1969) and Berry's (1968) formulations are introduced as special cases of a general description proposed in this section. The discussion also leads to alternative formulations.

In order to describe the autoconversion process phenomenologically, we pay attention to two aspects that are important in describing the autoconversion: a switch condition and a smooth monotonic increase of the rate with increasing cloud-water concentrations. First, autoconversion is inefficient when the cloud-water drop size is very small. Autoconversion becomes significant only after the droplets have grown above the radius of 20μm (cf., Ch. 8, Rogers and Yau, 1989). This is because, below this

ACPD
10, 30305–30345, 2010

radius, a sweeping section of cloud water is too small for making the autoconversion process efficient. A switch condition may be described by posing a threshold on the cloud-water concentration, assuming that the higher the concentration the larger the mean radius of droplets by following a similar argument to that which led to Eq. (3.9) for the raindrop size. Second, once the autoconversion process kicks in, the rate itself simply increases monotonically with increasing cloud-water concentrations in a much smoother manner.

We designate a threshold for a switch by $\rho_{c,r}$, and present the following formulation in terms of cloud-water content $\tilde{\rho}_c = \bar{\rho} q_c / \rho_{c,r}$ normalized by this threshold. We represent these two phenomenological aspects by multiplying two functions, say $S(\tilde{\rho}_c)$ and $f(\tilde{\rho}_c)$:

$$AUT = \frac{1}{\bar{\rho}} \tilde{k} S(\tilde{\rho}_c) f(\tilde{\rho}_c). \tag{4.2}$$

Here, $S(\tilde{\rho}_c)$ represents a switch, $f(\tilde{\rho}_c)$ a smooth monotonic increase, and $\tilde{k}$ is a constant factor. We assume that a universal formula $\tilde{k} S(\tilde{\rho}_c) f(\tilde{\rho}_c)$ for the autoconversion would be given in terms of the precipitating-water content, $\rho_c = \bar{\rho} q_c$, rather than the mixing ratio, q_c. By following the convention of the formulation in Sect. 3 given in terms of the mixing ratio, the universal formula $\tilde{k} S(\tilde{\rho}_c) f(\tilde{\rho}_c)$ is divided by the air density $\bar{\rho}$ in Eq. (4.2).

It is important to emphasize that the choice for the switch, $S(\tilde{\rho}_c)$, and the monotonic increase, $f(\tilde{\rho}_c)$, can be made independently each other. We develop a general type of phenomenologically autoconversion formulation in the following in this manner.

For switch, Kessler (1965, 1969) simply takes a step function:

$$S_K(x) = \mathcal{H}(x-1) \equiv \begin{cases} 0 & x < 1 \\ 1 & x > 1, \end{cases} \tag{4.3a}$$

whereas Berry (1968) adopts a much smoother function:

$$S_B(x) = \frac{x}{1+x}. \tag{4.3b}$$

ACPD
10, 30305–30345, 2010




Here, the subscripts K and B are added in order to distinguish between the Kessler and Berry schemes. Fig. 4 shows how S_B (long-dash) gradually transits from the non-activated state (zero) to the fully activated state (unity) compared to the sudden switch by S_K (solid).

The switch $S(x)$ can be generalized as

$$S(x) = \frac{x^\zeta}{1 + x^\zeta} \tag{4.3c}$$

with ζ an unspecified constant. The general formula (4.3c) reduces to Berry's for $\zeta = 1$, and to Kessler's for $\zeta \to +\infty$.

A smooth monotonically increasing function may simply be set as:

$$f(x) = x^{*\chi} \tag{4.4}$$

with a constant exponent χ. Here, we normally set $x^* = x$, but $x^* = x - 1$ is used when S_K is chosen as the switch in order to ensure continuity of the autoconversion rate over the threshold $x = 1$. Kessler chooses $\chi = 1$, whereas Berry chooses $\chi = 2$.

Putting these two choices together, the Kessler and Berry schemes are, respectively, given by

$$AUT_K = \frac{1}{\bar{\rho}} \tilde{k}_K (\tilde{\rho}_{c,K} - 1) \mathcal{H}(\tilde{\rho}_{c,K} - 1), \tag{4.5a}$$

$$AUT_B = \frac{1}{\bar{\rho}} \tilde{k}_B \frac{\tilde{\rho}_{c,B}^3}{1 + \tilde{\rho}_{c,B}}. \tag{4.5b}$$

Here constants are given by $\tilde{k}_K = k \rho_{c,r,K}$ and $\tilde{k}_B = \tilde{\alpha} \rho_{c,r,B}^2$ with $k = 10^{-3}$ 1/s, $\rho_{c,r,K} = 5 \times 10^{-4}$ kg/m^3, $\tilde{\alpha} = 3.34$, and $\rho_{c,r,B} = 5.082 \times 10^{-3}$ kg/m^3, or $\tilde{k}_K = 5 \times 10^{-7}$ kg/s/m^3 and $\tilde{k}_B = 8.63 \times 10^{-5}$ kg/s/m^3. Note that the Kessler and Berry schemes use different reference mixing ratios $\rho_{c,r,K}$ and $\rho_{c,r,B}$, and so the subscripts K and B have also been added to the normalized mixing ratio above for clarity.

ACPD
10, 30305–30345, 2010

As already emphasized above, both switch S and monotonic increase f functions are introduced independently in Kessler and Berry's formulations. Thus, it is legitimate to consider combinations crossing these two formulations.

A first choice is to take S_K as the switch function, with an exponent $\chi = 2$ in the monotonic function f as in the Berry scheme:

$$AUT_{KB} = \frac{1}{\bar{\rho}} \tilde{k}_K (\tilde{q}_{c,K} - 1)^2 \mathcal{H}(\tilde{q}_{c,K} - 1). \tag{4.5c}$$

An alternative is to take S_B as the switch function, with an exponent $\chi = 1$ in the monotonic function f as in the Kessler scheme:

$$AUT_{BK} = \frac{1}{\bar{\rho}} \tilde{k}_K \frac{\tilde{q}_{c,K}^2}{1 + \tilde{q}_{c,K}}. \tag{4.5d}$$

Here, in both cases, constants are chosen to be the same as for the Kessler scheme. We call these two schemes, Kessler-Berry and Berry-Kessler schemes, respectively. These four schemes for the autoconversion rate (Eq. 4.5a, b, c, d) are plotted in Fig. 5 with $\bar{\rho} = 1$ kg/m^3. Here, we see the reason for choosing the parameters of the Kessler scheme for the "mixed" schemes: they give better fit to the first two curves than those with the parameters for the Berry scheme. From a theoretical point of view, it would be of interest to investigate the role of the threshold as well, and thus we may simply set $\rho_{c,r} = 0$ in Kessler's formulation.

5 Tests with NAM-SCA

The four possible phenomenological description of autoconversion proposed in the last section are tested in the framework of the minimum bulk microphysical systems introduced in Sect. 2.2. These microphysics are implemented into a moist version of the nonhydrostatic anelastic model with segmentally–constant approximation (NAM–SCA) developed by Yano et al. (2010).

ACPD
10, 30305–30345, 2010

The model is based on a finite volume approach in the horizontal direction with a highly flexible mesh–adaptation capacity, essentially performed by following the vertical evolution of convective plumes. For details of the mesh–adaptation along with other model details, we refer to Yano et al. (2010). For the present purpose, a constant density fluid in the original study is replaced by an ideal gas with a gas constant for a standard dry atmosphere.

As in Yano et al. (2010), a two dimensional geometry is adopted with periodic boundary conditions in the horizontal direction. In the present tests, the horizontal domain size is set at 512 km with a maximum horizontal resolution $\Delta x = 2$ km and a minimum horizontal resolution $\Delta X = 256$ km. The model top is placed at 30 km with the vertical grid-size (full layer depth) gradually stretched from $\Delta z = 50$ m at the surface to $\Delta z = 1000$ m at the 20 km level. Above this level, a homogeneous vertical grid is used.

The model top boundary condition is changed from the original free surface to a rigid lid (with vanishing vertical velocity). The free–surface condition tends to make convection less organized and less coherent, although the difference is not dramatic. For this reason, results with the rigid-lid case are presented here. Note that no sponge layer is added to the uppermost levels even under this modification. By keeping the highest mesh-adaptation level to $z = 20$ km, well below the model top (30 km), wave reflection from the model top is not visible in the simulations.

As a test case, we adopt an idealized tropical squall–line experiment developed by Jung and Arakawa (2005). They defined an idealized steady "large–scale" forcing, $F_{1,\mathrm{LS}}$ and $F_{2,\mathrm{LS}}$, for the potential temperature and the moisture, respectively, based on GATE (Global Atmospheric Research Program (GARP) Atlantic Tropical Experiment) Phase-III mean observation. The "large–scale" forcing can formally be defined by

$$F_{1,\mathrm{LS}} = -\bar{\mathbf{v}} \cdot \nabla \bar{\theta} + \bar{Q}_R, \tag{5.1a}$$

$$F_{2,\mathrm{LS}} = -\bar{\mathbf{v}} \cdot \nabla \bar{q}_v. \tag{5.1b}$$

Here, all the variables with an overbar are "large-scale" means. More specifically, $\mathbf{v}$ is the *three-dimensional* wind velocity, and Q_R is the radiative heating rate. In deep

ACPD
10, 30305–30345, 2010

moist-convective modelling, as in the present case, these "large-scale" variables are typically estimated from synoptic–scale sounding network observations. In the present case, a time-independent idealized forcing defined by Jung and Arakawa (2005) based on the GATE Phase-III observation is adopted.

No extra "forcing" is added in the present set of simulations. Most importantly, no surface flux is included in the following simulations. Large–scale forcing defined by Jung and Arakawa (2005) is so strong that there is no necessity to add surface fluxes. te that, in the present study, their original forcing is slightly modified in such way that enthalpy of the system is conserved under the forcing.

Also note that, in the present test, the Lagrangian time-derivative is defined by

$$\frac{D}{Dt} = \frac{\partial}{\partial t} + (u + \bar{u})\frac{\partial}{\partial x}$$

where u (without overbar) designates the zonal wind explicitly computed within the NAM-SCA model, and $\bar{u}$ is a "large-scale" zonal wind as defined by Jung and Arakawa (2005), x is the eastward coordinate.

The model parameters are listed in the Appendix C. Adopted parameters are similar to those in Yano et al. (2010), but with adjustments for simulating mesoscale deep convection instead of boundary-layer dry convection as in the original work. As an additional major modification, only the first model layer is kept in the full resolution throughout the experiments, and mesh-refinement is applied in time to the second layer and those above. This modification contributes to a reduction of the "compression rate" of the simulation as seen below.

Snap shots of the evolution of the system are shown in Fig. 6 for the case with the Kessler scheme from the beginning of day 3 and with an interval of three hours. In these plots, the positions of the mesh–segment interfaces are indicated by vertical lines. It is seen that a westward-propagating squall–line system is successfully simulated by making intensive mesh refinements only within the convective regions. The dense-mesh region also shifts as the squall–line system propagates with time. Outside of the convective regions, almost no mesh refinement is applied, and the model

ACPD
10, 30305–30345, 2010

runs successfully with the minimum of two constant mesh–segments over the whole domain. The "compression rates" (defined as the ratio between the total number of mesh–segments and that with a full resolution) for these four frames are, in the order of the sequence shown: 0.127, 0.142, 0.116, and 0.109. The compression rates for other cases shown are comparable. Such values are almost half the best values achieved in the dry-convective boundary–layer simulations of Yano et al. (2010).

In order to summarize the dependence of the solution on the choice of the autoconversion scheme, the horizontal space–time section for the evolution of the precipitation field is shown in Fig. 7 for the four major choices of the autoconversion scheme. All of the cases gradually generate a westward-propagating convective system over a one-day period. Nevertheless, one may note that the case with the Kessler-Berry scheme (Fig. 7c) takes slightly longer to become organized. A noticeable defect of all cases is a lack of mesoscale stratiform rain, presumably due to the absence of ice microphysics. We refer to Zipser (1977) for an observational study (see especially his Fig. 13), and to Fovell and Ogura (1988) for a modelling study.

Also note the highly "digitalized" nature of the simulations. In particular, a notable discontinuity in the physical fields at $x = 256$ km is due to a fixed segment interface posed as the minimum resolution. The precipitation field in Fig. 7 is often, outside the convective region, almost horizontally homogeneous at both sides of this interface, because only these two mesh segments are found at many vertical levels as indicated by the distributions of segment interfaces in Fig. 6.

Another way of summarizing the differences between these four choices of the autoconversion scheme is the snap shot of the simulations shown in Fig. 8 for day five: the Berry scheme (b) develops the most extensive stratiform deck, and the second best is the Berry–Kessler scheme (d). It may be important to emphasize that the stratiform deck can be developed without ice microphysics, although the amount of associated precipitation is limited.

All of the schemes suffer from a tendency to fill out the upper levels (above 8 km) with a thin "fog" of the order $q_c \sim 10^{-1}$ g/kg. The problem is most serious with the Berry

ACPD
10, 30305–30345, 2010

scheme, and the least serious with the Berry–Kessler scheme. Furthermore, the two cases (Kessler and Kessler-Berry: a, c) adopting the Kessler "switch", S_K, (Eq. 4.3a) suffer from a lack of stratiform clouds with a deep convective tower directly embedded into a model–domain spread of "fog". We attribute the formation of "fog" to the absence of ice in the microphysics. We expect that such "fog" would be rapidly removed if ice were to be formed within the "fog" layer.

As an additional case, we consider a Kessler scheme without threshold defined by

$$AUT_{Kn} = \frac{1}{\bar{\rho}} \tilde{k}_K \tilde{\rho}_{c,K} . \tag{5.2}$$

The result is shown in Fig. 9 in the same format as in Fig. 6. The most striking effect of removing the threshold in the Kessler scheme is an almost total removal of the upper-level "fog" with a slight indication of a tendency for forming a stratiform deck.

One of the main aspects discussed is the capability of a scheme to generate an extensive stratiform deck. Comparison of the four schemes in Fig. 8 suggests that the use of a smooth switch as adopted by the Berry scheme is key for such a capability. In this respect, the contrast between the Berry and Kessler–Berrry schemes may be worthwhile to notice. This is remarkable, especially considering the closeness of the autoconversion curves of these two schemes as shown in Fig. 5.

6 Conclusions

A short comparison analysis here shows a strong dependence of the simulation of a mesoscale convective system on the bulk autoconversion scheme. A more extensive analysis could be performed using the generalized form of the autoconversion formula as given by Eqs. (4.3c) and (4.4). However, before we further pursue such a systematic analysis, two major issues must be resolved. First is the development of a methodology for better elucidating the sensitivity of the convective system to the choice of bulk microphysics. This issue includes the development of a simpler dynamical model that

ACPD
10, 30305–30345, 2010

would make such an analysis more tractable and transparent. Moncrieff 's (1981, 1992) archetypal model may provide a prototype for this purpose. Another possibility could be a much idealized two–cylinder system such way that considered by Ogura and Takahashi (1971). The second issue is the need for a more systematic methodology for developing and verifying a phenomenological description of microphysical processes from more basic physical principles. Berry's (1968) classical work that derives such a phenomenological description from a numerical result of a more complete theoretical model may give a good guidance for this purpose.

Appendix A List of numerical values for parameters

A1 Eq. (3.2): Marshall-Palmer distribution

The constant n_0 is observationally estimated to be in the range of $n_0 = 0.3\text{–}1 \times 10^7\ \mathrm{m}^{-4}$ (Gunn and Marshall, 1958; Joss et al., 1968; Joss and Waldvogel, 1969; Sekhon and Srivastava, 1971). The most commonly used choice is $n_0 = 10^7\ \mathrm{m}^{-4}$ (cf., Grabowski , 1998). The present implementation also adopts this value.

A2 Terminal velocity (Sect. 3.2.1):

According to Kessler (1969) and Grabowski (1988):

$$\tilde{v} = 130, d = 0.5$$

This leads to the factor in Eq. (3.18):

$$\Gamma(b+d+1)/\Gamma(b+1) = 1.9386$$

A3 Accretion (Sect. 3.2.2):

According to Grabowski (1998), the basic parameters are:

$$E = 0.8, \quad \alpha = 1.$$

ACPD
10, 30305–30345, 2010

In general, the value of α sensibly depends on a shape of ice crystals, and notably $\alpha \ll 1$ for needles.

With the parameters already defined above,

$$\frac{d+3}{b+1} = 0.875$$

It suggests $(d+3)/(b+1) \simeq 1$ is a good approximation. That furthermore leads to

$$\Gamma(d+3) = 3.323$$

$$(ACC)_0 = 1.773 \mathrm{m}^3/\mathrm{kg/sec}$$

A4 Eq. (3.25): Re-evaporation

- Table 7.1 of Rogers and Yau (1989) lists the values of μ, D_v, and the thermal diffusivity k as functions of the temperature.
- Ventilation factor F: Values adopted in Grabowski (1988) are $F_0 = 1.0$, $\psi = 0.22$, $l = 1$, whereas Grabowski (1998) proposes to use $F_0 = 0.78$, $\psi = 0.27$, $l = 2$.

Appendix B Gamma function

The Gamma function is defined by

$$\Gamma(x) = \int_0^{+\infty} \xi^{x-1} e^{-\xi} d\xi. \tag{B.1}$$

A rather obvious, but frequently quoted formula in the text is

$$\int_0^{+\infty} (\lambda D)^{x-1} e^{-\lambda D} dD = \frac{1}{\lambda} \Gamma(x). \tag{B.2}$$

ACPD
10, 30305–30345, 2010

The followings properties for the Gamma function are also used in the main text and Appendix A:

$$\Gamma(1) = 1,$$

$$\Gamma(x+1) = x\Gamma(x).$$

Note especially $\Gamma(n+1) = n!$ when n in an integer.

Appendix C Model parameters

Here, the model parameters are listed with the values adopted. See Yano et al. (2010) for the precise definitions of the parameters.

C1 Model resolution related parameters:

$L = 512$ km: horizontal domain size
$H = 30$ km: top height of the model
$N_x = 256$: total number of mesh segments under a full resolution
$N_z = 50$: total number of full vertical levels
$M_x = 2$: minimum number of mesh segments allowed at each vertical level
$\Delta t = 5$ s: time step (default)
1 s: time step for *list the cases here*
$\Delta X = 256$ km: length of the mesh segment under the minimum resolution
$\Delta x = 2$ km: full horizontal resolution

C2 Critical vertical levels:

$k_b = 1$: maximum height at which the full resolution is always maintained
$k_m = 20$: top height at that the full resolution is initially introduced (5.4 km height)

ACPD
10, 30305–30345, 2010

$k_t = 40$: maximum height level (20 km height) at which activation and deactivation of mesh segments is performed. Above this level, the minimum resolution M_x is always maintained

C3 Vertical depth for performing activation and deactivation:

$\Delta k_a = 3$: vertical depth over which activation is performed

$\Delta k_d = 0$: vertical depth over which the deactivation condition is checked

C4 Intervals for activation and deactivation

$n_a = 10$: interval for performing activation given as a number of time steps

$n_d = 10$: interval for performing deactivation given as a number of time steps

C5 Relative thresholds for activation and deactivation:

$\gamma_a = 1.0$: threshold for activation relative to the standard deviation at a given vertical level

$\gamma_d = 1.0$: threshold for deactivation relative to the standard deviation at a given vertical level

$\gamma_{\min} = 0.1$: threshold for activation and deactivation relative to the total standard deviation

Acknowledgements. The present work is performed under a framework of COST Action ES0905. Discussions with Wojciech Grabowski are greatly appreciated. He also provided us forcing data for Jung and Arakwa's test case. Careful reading of the text by R. S. Plant is acknowledged.

ACPD

10, 30305–30345, 2010

The publication of this article is financed by CNRS-INSU.

References

Asai, T.: A numerical study of the air–mass transformation over the Japan Sea in winter, J. Meteor. Soc. Jpn., 43, 1–15, 1965. 30310

Berry, E. X.: Modification of the warm rain process, Proc. First Conf. on Weather Modification, Albany, NY, Amer. Meteor. Soc., 81–85, 1968. 30322, 30323, 30330

Biello, J. A., Majda, A. J., and Moncrieff, M. W.: Meridional momentum flux and superrotation in the multiscale IPESD MJO model, J. Atmos. Sci., 64, 1636–1651, 2007. 30306

Fovell, R. G. and Ogura, Y.: Numerical simulation of a midlatitude squall line in two dimensions, J. Atmos. Sci., 45, 3846–3879, 1988. 30328

Grabowski, W. W.: On the bulk parameterization of snow and its application to the quantitative studies of precipitation growth, PAGEOPH, 127, 79–92, 1988. 30310, 30330, 30331

Grabowski, W. W.: On the influence of small–scale topography on precipitation, Q. J. Roy. Meteorol. Soc., 115, 633–650, 1989. 30310

Grabowski, W. W.: Towards cloud resolving modelling of large-scale tropical circulations: A simple cloud microphysics parameterization, J. Atmos. Sci., 55, 3283–3298, 1998. 30307, 30316, 30318, 30330, 30331, 30338, 30339

Gunn, K. L. S. and Marshall, J. S.: The distribution with size of aggregate snowflakes, J. Meteorol., 15, 452–461, 1958. 30330

Held, I. M.: The gap between simulation and understanding in climate modeling, B. Am. Meteorol. Soc., 86, 1609–1614, 2005. 30307

Joss, J. and Waldvogel, A.: Raindrop size distribution and sampling size errors, J. Atmos. Sci., 26, 566–569, 1969. 30330

Joss, J., Tham, J. C., and Waldvogel, A.: Reprints Cloud Physics Conference, Toronto, University of Toronto Press, Toronto, Canada, p. 369, 1968. 30330
Jung, J.-H. and Arakawa, A.: Preliminary tests of multiscale modeling with a two–dimensional framework: Sensitivity to coupling methods, J. Atmos. Sci., 133, 649–662, 2005. 30326, 30327
Kessler III, E.: Microphysical parameters in relation to tropical cloud and precipitation distributions and their modifications, Geofisica International, July 1975, 5(3), 79–88, 1965. 30307, 30322, 30323
Kessler III, E.: On the Distribution and Continuity of Water Substance in Atmospheric Circulations, Meteor. Monogr., Amer. Meteor. Soc., 32, 84 pp., 1969. 30307, 30322, 30323, 30330
Khain, A., Pokrovsky, A., Pinsky, M., Seifert, A., and Phillips, V.: Simulation of effects of atmospheric aerosols on deep turbulent convective clouds using a spectral microphysics mixed-phase cumulus cloud model. Part I: Model description and possible applications, J. Atmos. Sci., 61, 2963–2982, 2004. 30306
Khouider, B., and Majda, A. J.: A simple multicloud parameterization for convectively coupled tropical waves. Part I: Linear analysis. J. Atmos. Sci., 63, 1308–1323, 2006. 30306
Khouider, B., and Majda, A. J.: A simple multicloud parameterization for convectively coupled tropical waves. Part II: Nonlinear simulations J. Atmos. Sci., 64, 381–400, 2007. 30306
Lopez, P.: Implementation and validation of a new prognostic large-scale cloud and precipitation scheme for climate and data-assimilation purposes, Q. J. Roy. Meteorol. Soc., 128, 229–257, 2002. 30320
Majda, A. J.: Multiscale models with moisture and systematic strategies for superparameterization, J. Atmos. Sci.,, 2726–2734, 2007a. 30306
Majda, A. J.: New multiscale models and self-similarity in tropical convection, J. Atmos. Sci., 64, 1393–1404, 2007b. 30306
Marshall, J. S., and W. M. Palmer: The distribution of raindrops with size, J. Meteorol., 5, 165–166, 1948. 30312, 30313
Moncrieff, M. W., 1981: A theory of organized steady convection and its transport properties, Q. J. Roy. Meteor. Soc.,107, 29–50, 1981. 30330
Moncrieff, M. W.: Organized convective systems: Archetypal dynamical models, mass and momentum flux theory, and parameterization, Q. J. Roy. Meteorol. Soc., 118, 819–850, 1992.
Morrison, H., J. A. Curry, M. D. Shupe, and Z. Zuidema: A new double–moment microphysics parameterization for application in cloud and climate models. Part II: Single-column mod-

ACPD
10, 30305–30345, 2010

elling of arctic clouds, J. Atmos. Sci., 62, 1678–1693, 2005. 30306
Ogura, Y., and T. Takahashi: Numerical simulation of the life cycle of a thunderstorm cell. Mon. Weather Rev., 99, 895–911, 1971. 30330
Phillips, V. T. J., Blyth, A. M., Choularton, T. W., Brown, P. R. A., and Latham, J.: The glaciation of a cumulus cloud over New Mexico, Q. J. Roy. Meteorol. Soc., 127, 1513–1534, 2001. 30306
Pruppacher, H. R. and Klett, J. D.: Microphysics of Clouds and Precipitation, Second Revised and Enlarged Edition with an Introduction to Cloud Chemistry and Cloud Electricity, Kluwer Academic Publisheres, Dordrecht, The Netherlands, 954 pp., 1997. 30306, 30319, 30322
Rogers, R. R. and M. K. Yau: Short Course in Cloud Physics, 3rd Ed., Pergamon Press, 290 pp., 1989. 30306, 30319, 30322, 30331
Rutledge, S. A. and Hobbs, P. V.: The mesoscale and microscale structure of clouds and precipitation in midlatitude cyclones. VIII: A model for the 'seeder–feeder' process in warm-frontal rainbands, J. Atmos. Sci., 40, 1185–1206, 1983. 30310
Seifert, A. and Beheng, K. D.: A double-moment parameterization for simulating autoconversion, accretion and selfcollection. Atmos. Res., 59–60, 265–281, 2001. 30322
Sekhon, R. S. and Srivastava, R. C.: Doppler radar observations of drop-size distributions in a Thunderstorm, J. Atmos. Sci., 28, 983–994, 1971. 30330
Yano, J.-I.: Diffusion Growth and Evaporation of Water Drops and Snow Crystals, technical notes. avaialble at: ftp://cnrm-ftp.meteo.fr/pub-moana/yano/publication/diff.pdf, 2010. 30319
Yano, J.-I., Benard, P., Couvreux, F., and Lahellec, A.: NAM-SCA: Nonhydrostatic Anelastic Model under Segmentally–Constant Approximation, Mon. Weather Rev., 138, 1957–1974, 2010. 30308, 30325, 30326, 30327, 30328, 30332
Yau, M. K. and P. M. Austin: A model for hydrometer growth and evolution of raindrop size spectra in cumulus cells, J. Atmos. Sci., 36, 655–668, 1979. 30310
Zipser, E. J.: Mesoscale and Convective–Scale Downdrafts as Distinct Components of Squall-Line Structure, Mon. Weather Rev., 105, 1568–1589, 1977. 30328

ACPD
10, 30305–30345, 2010

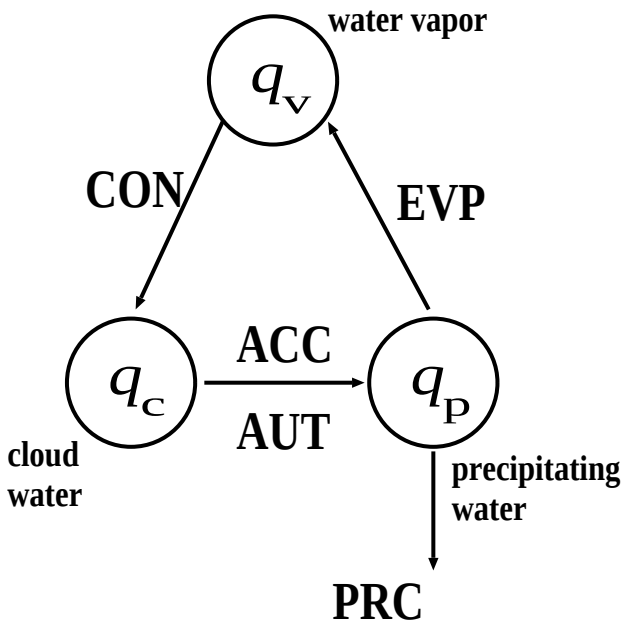

Fig. 1. Conversion cycle of the microphysics considered.

ACPD
10, 30305–30345, 2010




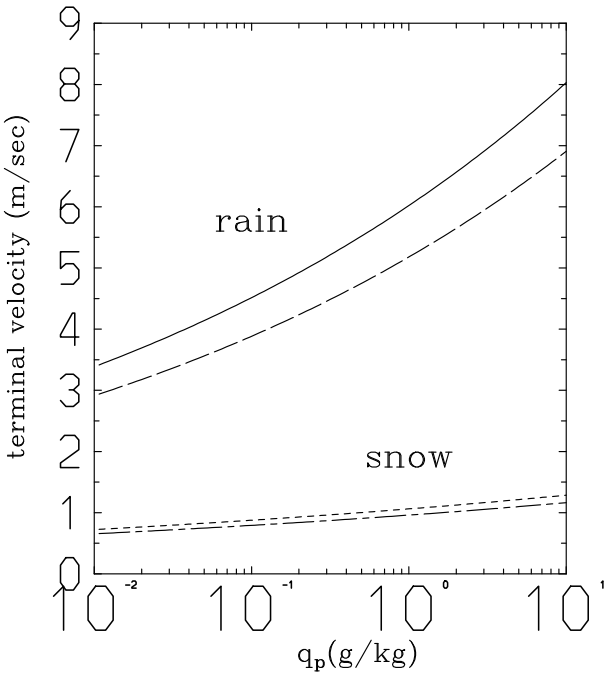

Fig. 2. The terminal velocity v_T^* (Eq. 3.18) plotted as a function of the precipitating-water mixing ratio q_p. Plotted are for the two extreme limits for the particle number $n_0 = 3 \times 10^6\ \mathrm{m}^{-4}$ (solid) and $n_0 = 10^7\ \mathrm{m}^{-4}$ (long-dash: cf., Appendix A1). The curves for the snow are also shown by short-dash and chain-dash curves, respectively,with standard parameters (cf., Grabowski , 1998).

ACPD
10, 30305–30345, 2010

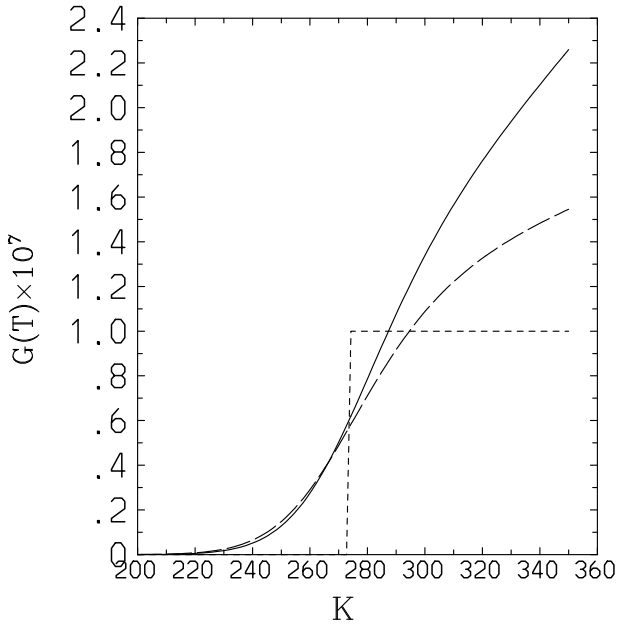

Fig. 3. The thermodynamic function $G(T)$ (Eq. 3.26) as a function of the temperature. Also shown by a dashed curve is an approximation (Eq. 3.27) proposed by Grabowski (1998). The short–dashed curve is the proposed approximation (Eq. 3.32).

ACPD
10, 30305–30345, 2010

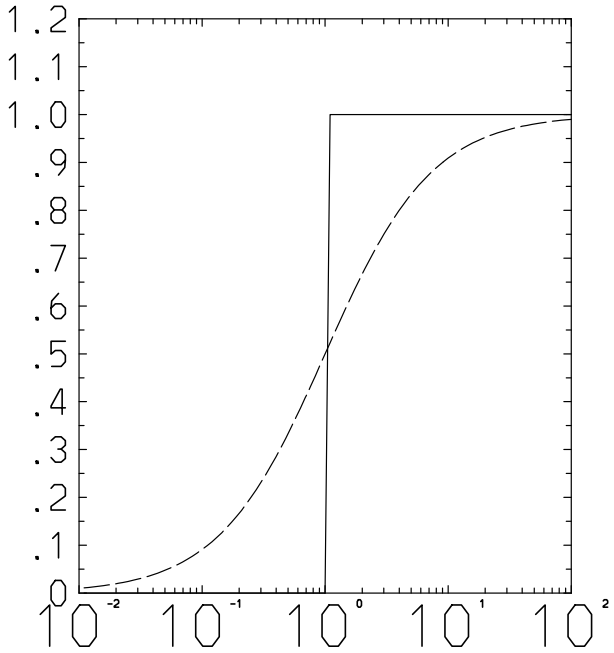

Fig. 4. Two choices of the switch function: a sudden switch (4.3a: solid) and a gradual switch (4.3b: long–dash).

ACPD
10, 30305–30345, 2010

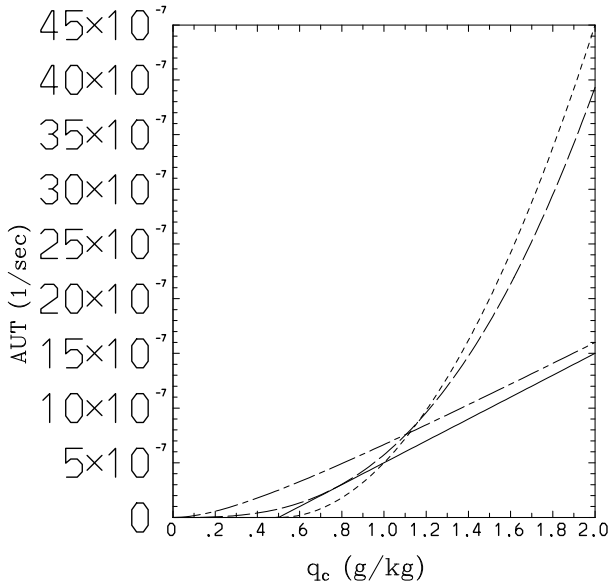

Fig. 5. Four possible autoconversion formulae are plotted as functions of the cloud-water mixing–ratio, q_c: Kessler, Eq. (4.5a: solid); Berry, (4.5b: long–dash); Kessler–Berry (4.5c: short–dash); Berry-Kessler (4.5d: chain–dash).

ACPD
10, 30305–30345, 2010

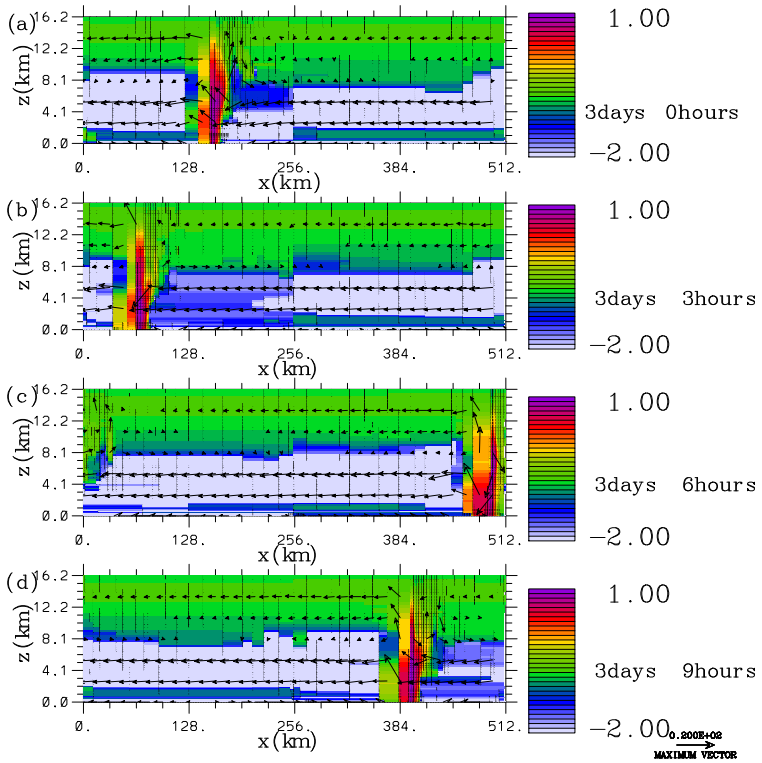

Fig. 6. The total condensate, $q_c + q_p$, are shown by color shade in logarithmic scale for the range from 10^{-2} g/kg to 10 g/kg as defined by a color code to the right. The vectors show the winds with unit of 20 m/sec and 2 m/sec for the horizontal and the vertical components, respectively. The unit vector length is shown at the bottom right. The interfaces between the model mesh–segments are indicated by vertical lines. Note that the model top is at 30 km, whereas only the lowest 16.2 km are shown here.

ACPD
10, 30305–30345, 2010

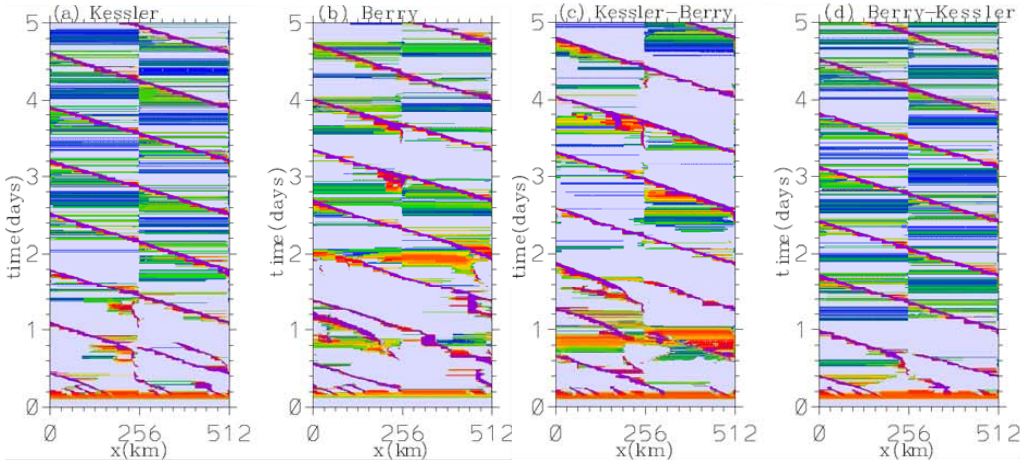

Fig. 7. The horizontal space–time section for the evolution of the precipitation field for the first five days of the simulations. The cases shown are with **(a)** Kessler, **(b)** Berry, **(c)** Kessler-Berry, and **(d)** Berry-Kessler schemes. The range of color shade is from 10^{-2} mm/hour to 10 mm/hour in logarithmic scale with the color code as defined in Fig. 6.

ACPD
10, 30305–30345, 2010

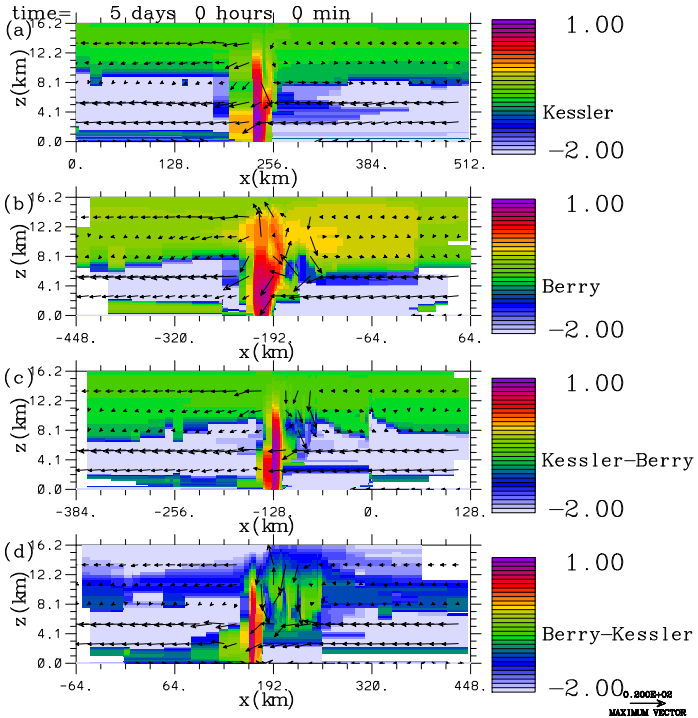

Fig. 8. A snap shot of simulations on the day five for the four choices of the autoconversion scheme: **(a)** Kessler, **(b)** Berry, **(c)** Kessler-Berry, and **(d)** Berry-Kessler schemes. The total condensate, $q_c + q_p$, and the wind vectors are shown by color shade and vectors in the same format as in Fig. 6. The vertical lines for indicating the mesh–segment interfaces are omitted here. Note that the horizontal coordinates are shifted in order to place the squall–line system to a center of the frame.

ACPD
10, 30305–30345, 2010

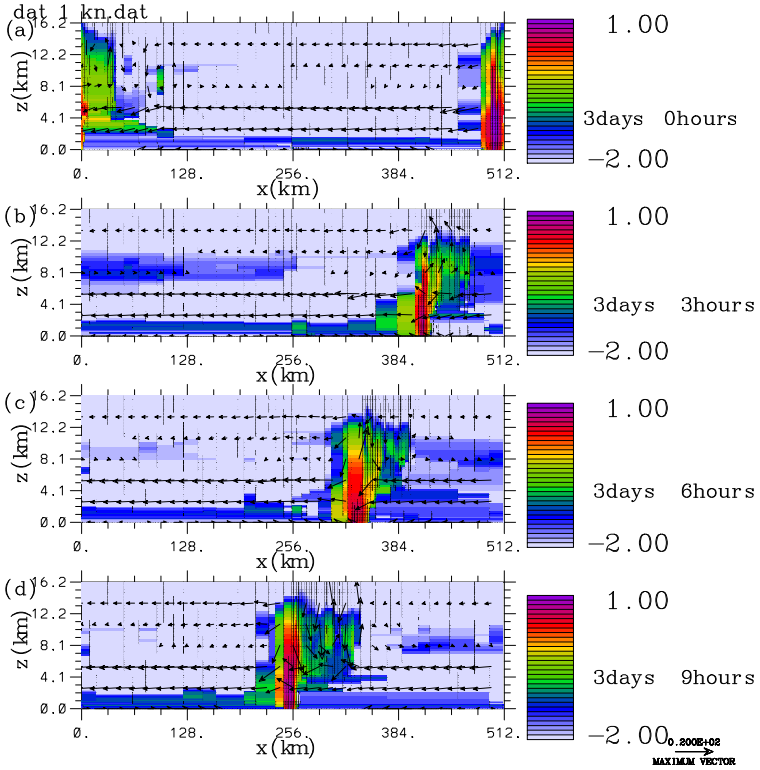

Fig. 9. The same as for Fig. 6 but with the the Kessler scheme without threshold.

ACPD
10, 30305–30345, 2010